Luminescence from hot carrier interband recombination in wide InGaN quantum wells

Conny Becht [1], Lukas Uhlig [1], Mateusz Hajdel [2], Grzegorz Muziol [2] and Ulrich T. Schwarz [1,*]

[1] *Institute of Physics, Chemnitz University of Technology, 09126 Chemnitz, Germany*

[2] *Institute of High Pressure Physics, Polish Academy of Sciences, 01-142 Warsaw, Poland*

(Received 1 July 2025; revised 18 September 2025; accepted 30 September 2025; published 23 October 2025)

Direct radiative recombination of high excited confined states across the band gap is observed as a broad emission band above the InGaN band edge in photoluminescence and electroluminescence for wide InGaN quantum wells (QWs). The observation of hot carrier interband recombination is possible in wide InGaN quantum wells because the transitions between the lower lying confined states are spatially indirect due to the piezoelectric field, and therefore become dark states with extremely low radiative transition rates at low carrier densities. Hot carrier luminescence was observed consistently for 7.8- and 25-nm-wide QWs at low and room temperature, while it is absent for a 2.6-nm-thin QW. The spectrum of the emission is explained by $k \cdot p$ simulations assuming a weak dependency of the transition matrix element on the subband of the confined states, and a limited extent of carrier momentum around the Γ point.

DOI: 10.1103/5x2d-jdly

I. INTRODUCTION

Semiconductor heterostructures and in particular quantum wells (QWs) enable efficient optoelectronic devices [1,2], most notably thin quantum wells with thickness $d \approx 3$ nm in light emitting diodes (LEDs) and laser diodes (LDs) [3–5]. QWs allow tuning of the emission energy, avoiding reabsorption, and tailoring the carrier density for maximized internal quantum efficiency (IQE). Moderately wide InGaN QWs ($d \approx 8$ nm) are used to boost the internal quantum efficiency for blue LEDs by reducing the carrier density and therefore Auger-Meitner nonradiative recombination [6–11]. Recently, efficient wide well ($d > 15$ nm) LEDs and LDs with high differential gain were demonstrated, using plasma-assisted molecular beam epitaxy (PAMBE) [12]. These wide InGaN quantum wells display interesting physical behavior.

Electrons and holes are injected from transport layers and barriers with a higher band gap into the confined energy states of the QW. Carrier capture and intraband relaxation from the transport layer into the thermal equilibrium of the confined states in the QW happens on a picosecond timescale [13–15], which is very fast compared to the nanosecond timescale for interband radiative and nonradiative recombination [16,17]. Therefore, the electron and hole densities are given by two distinct thermal Fermi-Dirac distributions in the conduction and valence band with respective quasi-Fermi levels. The energy distribution of radiative recombination follows approximately the combined occupation density of electrons and holes, the product of the Fermi-Dirac distributions, and inhomogeneously broadened density of states, resulting in emission at the band edge.

In stark contrast to this, we observe the appearance of a spectrally broad emission band several 100 meV above the ground state interband transition in wide InGaN quantum wells, observable both in photoluminescence (PL) and electroluminescence (EL). We interpret this emission as originating from hot carriers which are not relaxed to the equilibrium of the respective band. The physical reason why this emission can be observed in wide InGaN QWs is the "dark state" character of lower-energy states at low carrier density. The situation is shown in Fig. 1, where wave functions of the confined states of a 7.8-nm-thick InGaN QW are plotted for two different carrier densities. The strong piezoelectric field in strained InGaN QWs [16,18–22] causes a tilted QW potential and consequently a reduced electron-hole wave-function overlap [see Fig. 1(a)]. In particular, the center of gravity of the electron and hole ground states becomes separated spatially by approximately the width of the QW, in the direction of the piezoelectric field. For a wide QW with a strong field, this separation becomes large when compared to the spread of the respective wave functions, resulting in a very small transition matrix element and radiative recombination times from microseconds to milliseconds [23,24]. The wave-function overlap for higher-energy states is less affected by the band edge tilt and is thus large. Due to the electric field, all interband transitions are symmetry allowed [25].

At high carrier densities [Fig. 1(b)], within the typical range for LED or laser diode operation, the piezoelectric field inside the QW is mostly screened. While there may still be a low density of dark states in the corners of the QW, there is a high density of states with a low confinement energy and large wave-function overlap. Intraband carrier relaxation from the barrier level to the thermalized confined state happens on the picosecond timescale [13]. In the screened case, radiative and

*Contact author: ulrich.schwarz@physik.tu-chemnitz.de

Published by the American Physical Society under the terms of the Creative Commons Attribution 4.0 International license. Further distribution of this work must maintain attribution to the author(s) and the published article's title, journal citation, and DOI.

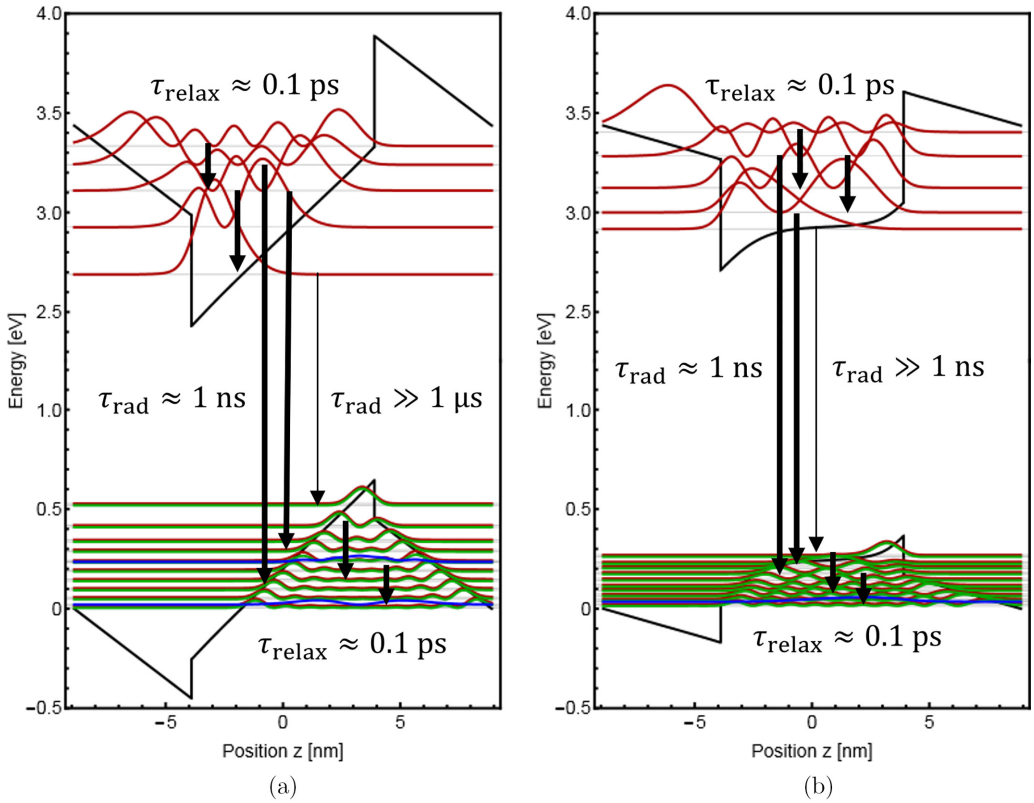


FIG. 1. Valence and conduction band edge for a 7.8-nm-wide QW for (a) low carrier density $n = 10^{12}$ cm^{-2} and (b) higher carrier density 10^{13} cm^{-2}; band edge and wave functions are calculated by self-consistent Schrödinger-Poisson and $k \cdot p$ simulations; transition rates are indicated schematically.

nonradiative interband recombination are on the nanosecond timescale [17,26]. Consequently, radiative emission from the hot carriers of transition states is negligible compared to the bright band edge emission.

In the case of low carrier density [Fig. 1(a)], the intraband relaxation process remains fast for all transitions above the band edge. As before, only a small fraction of the hot carriers recombines radiatively, while most relax to the thermal equilibrium. The quasi-Fermi level is far below the band edge and carrier density is low despite the long radiative carrier lifetime, because carriers are extracted from confinement energy states by nonradiative recombination and lateral diffusion. In this situation, the luminescence from the low density of hot carriers in nonequilibrium states with nanosecond recombination time can be stronger than the luminescence from carriers in equilibrium near the band edge, with a higher but still low carrier density but an extremely long radiative recombination time constant. In this situation it becomes possible to observe the spectrally broad emission from the continuum of higher-energy levels.

In the experiment, to be discussed in detail in the following section, the photoluminescence from hot carriers shows up as a broad band around $\lambda = 444$ nm, well above the band edge of the screened wide QW at $\lambda = 455$ nm. This feature is absent in the thin QW (see Fig. 2). In a small range of excitation densities, photoluminescence from hot carriers and from the wide QW can be observed simultaneously as two distinct peaks. We will show that the spectra correspond to theoretical expectations with two basic assumptions: Carrier distribution corresponds to a flow equilibrium with the energy-independent occupation of states, however limited to a range of momentum states in the vicinity of the Γ point.

A related observation of excited-state emission was discussed in photochemistry as the anti-Kasha effect [27]. However, there the emission was caused by an unusually fast radiative transition from excited states. In contrast to this, in the semiconductor QW system the transition between states of the quasiequilibrium distributions is masked as they become dark states.

The observation of emission from hot electron interband transitions contributes to the fundamental understanding of recombination in III-nitride semiconductor QWs. Hot carriers generated by the Auger-Meitner effect allowed for the first time the direct observation of Auger-Meitner recombination as the dominant mechanism for the efficiency droop in InGaN QW LEDs [28,29]. There, the hot electrons were above the barrier layer band edge and observed by electron emission from the cesiated semiconductor surface. Furthermore, emission from hot electrons was also observed in the high fields of lateral AlGaN high electron mobility transistors (HEMTs) when the channel is close to cutoff [30,31]. The signature is a Maxwell distribution of the bremsstrahlung emission of hot electrons relaxing to the band edge. In contrast to these two cases of hot electron emission, we observe the transitions between the continuum of high-energy states confined within InGaN QWs, thus contributing to the understanding

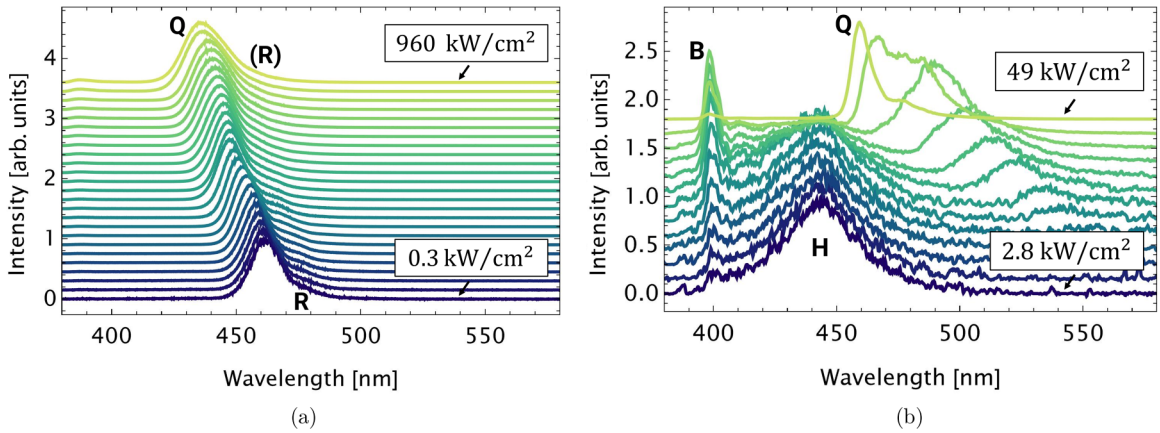


FIG. 2. PL spectra at $T = 10$ K for different excitation densities for the (a) 2.6-nm- and (b) 7.8-nm-wide QW (samples PL2.6nm and PL7.8nm, respectively). The spectra are normalized and shifted vertically for clarification. Components of the emission spectrum are marked as B: barrier, H: hot carrier, Q: quantum well, R: phonon replica. The excitation power in (a) is 0.3 kW/cm$^2 \cdot 1.54^i$ with $i = 0, 1, 2, \ldots, 11$ for the first 12 spectra and 33.3 kW/cm$^2 \cdot 1.32^i$ with $i = 0, 1, 2, \ldots, 12$ for the remaining spectra and in (b) 2.8 kW/cm$^2 \cdot 1.27^i$ with $i = 0, 1, 2, \ldots, 12$.

of carrier capture and intraband relaxation in optoelectronic devices.

II. EXPERIMENTAL OBSERVATION OF HOT CARRIER EMISSION

For this study we compare PL and EL spectra of two sets of three samples with a single QW of 2.6, 7.8, and 25 nm thickness. One set was a full LED structure with a *pn* junction and electrical contact for EL investigations, and the other set was with single QWs between $In_{0.02}Ga_{0.98}N$ barriers for PL excitation. We refer to the samples as EL2.6nm, EL7.8nm, EL25nm, PL2.6nm, PL7.8nm, and PL25nm, respectively. All samples are grown by plasma-assisted molecular beam epitaxy (PAMBE), and details on growth and the wide QW samples series are provided in Refs. [10,32].

The μPL and μEL measurements were performed with a confocal microscope using a continuous-wave excitation laser with 375 nm wavelength (iBeam Smart from Toptica Photonics AG), an objective with magnification of 63× and a high numerical aperture of 0.75 (Zeiss LD Plan-Neofluar). Excitation power density was controlled by a variable density filter wheel. The excitation spot radius was 250 nm [33]. A Keithley 2400 source meter was used as the current source for EL. The luminescence is collected by a single mode fiber with core diameter of 10 μm and the light is analyzed by a 55-cm focal length spectrometer (iHR-550 from Horiba) combined with a back-illuminated CCD detector (Synapse BIVS from Horiba, thermoelectric cooling, 2048 × 512 pixels with 13.5 µm pitch). The spatial resolution is as high as 200 nm and limited by diffraction. For low-temperature studies the samples are mounted inside a KONTI Micro continuous-flow cryostat from CryoVac GmbH cooled with liquid helium. The temperature is controlled with a TIC-500 cryogenic temperature controller in the 4–400 K range.

PL spectra at different excitation densities for a 2.6-nm-thin QW (sample PL2.6nm) at a cryogenic temperature of $T = 10$ K are shown in Fig. 2(a) as a reference. As the excitation power and consequently the charge carrier density increases, a blueshift of the peak emission is observed, and at higher excitation densities also a broadening of the spectra. The blueshift is caused by screening of the quantum-confined Stark effect and band filling due to charge carrier injection, partially compensated by band gap renormalization [20,21]. The excitation power covers the Shockley-Read-Hall nonradiative, peak IQE, and nonradiative Auger-Meitner regimes of the IQE curve. The broadening is caused by band filling in the degenerate case, when the energy of the quasi-Fermi level is close to the band edge. Band renormalization is reducing the blueshift at high carrier densities. The shoulder on the low-energy side, also known as phonon replica, is explained by the emission of longitudinal optical (LO) phonons [34]. At low excitation densities the QW band edge is tilted due to the piezoelectric field, and the wave-function overlap is reduced, but not enough to suppress ground state radiative recombination.

The corresponding set of spectra for the 7.8-nm-thick QW (sample PL7.8nm) at $T = 10$ K is plotted in Fig. 2(b). The emission by electron-hole recombination from carriers of the states in quasiequilibrium in the respective band results in the peak at the longest wavelengths, shifting from about 540 nm at the lowest excitation to 459 nm at the highest excitation. This extremely large blueshift of about 81 nm (0.41 eV) is indicative of the large quantum-confined Stark effect in the wide QW. At intermediate excitation densities, the PL line shows a substructure, corresponding to transitions between different excited states [10,11].

Two separate peaks on the high-energy side dominate the PL7.8nm spectrum at low excitation densities. Both peaks are above the band edge of the fully screened QW (448 nm at low temperature). The peak at 400 nm is caused by the $In_{0.02}Ga_{0.98}N$ barrier emission [35]. We attribute the broad peak at 444 nm to hot carrier emission. This broad line peaks at higher energies than the 459 nm band edge of the fully screened QW. Furthermore, in this low excitation density range, emission from band-edge states are redshifted beyond 540 nm or disappears, as these states are dark. Within a cer-

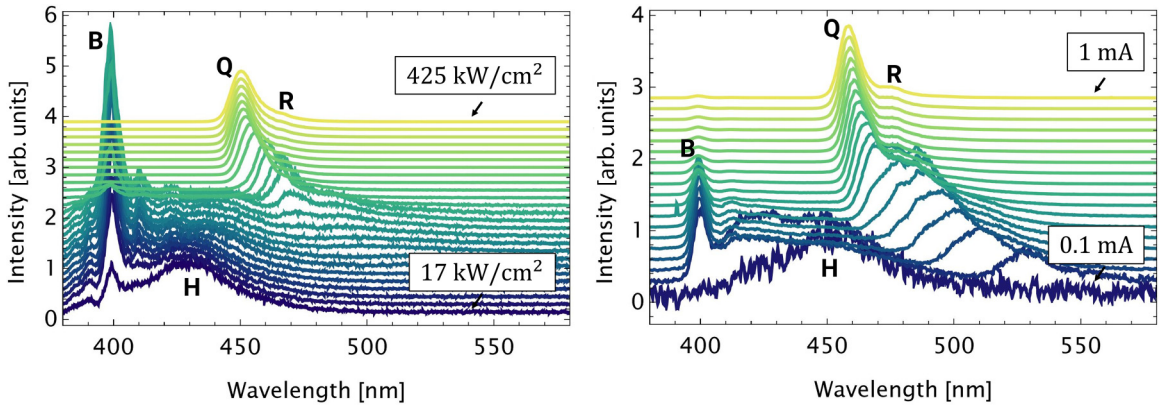


FIG. 3. (a) PL spectra and (b) EL spectra of a 7.8-nm-wide QW, both at $T = 10$ K. The spectra are normalized and vertically shifted for clarification. Components of the emission spectrum are marked as B: barrier, H: hot carrier, Q: quantum well, R: phonon replica. The excitation power in (a) is 17, 41, 45, 53, 60, 70, 80, 88, 103, 106, 112, 119, 123, 127, 137, 150, 158, 183, 198, 229, 260, 295, 326, 356, 389, 425 kW/cm^2 for the respective spectrum and the current in (b) is from 0.1 to 1 mA in 0.05 mA steps.

tain range of excitation densities, the emission from hot and thermalized carriers is visible as two distinct peaks. In these cases the energy separation between the ground state emission and hot carrier emission is about 90 nm (0.45 eV).

Luminescence from hot electrons is visible in EL as well, as shown by the comparison of PL [Fig. 3(a)] and EL [Fig. 3(b)] at $T = 10$ K for the PL7.8nm and EL7.8nm sample, respectively. For the PL spectra the range of excitation was extended to 425 kW/cm^2, when compared to Fig. 2(b). At the highest carrier densities, no significant wavelength shift is observed and the spectra just broaden, i.e., the internal fields are completely screened and band filling is responsible for the spectral broadening. When the internal field is screened, the confined states of the wide QW are closely spaced, resulting in a bulklike high density of states [11]. EL and PL spectra exhibit consistent behavior: a strong Stark shift at low carrier densities; decrease of the emission from thermalized states at low carrier densities (dark states); a stable peak at the band edge of the screened QW at high carrier densities; a barrier emission at 400 nm; and broad emission from hot carriers in the spectral region between thermalized confined states and barrier states. The internal fields of the *pn* junction in the biased EL structure and the unbiased PL sample without a *pn* transition differ in the band edge profile across the active region and carrier injection, which is responsible for the remaining differences between PL and EL spectra.

Hot carrier emission from a 25-nm-wide QW (sample PL25nm) was measured with PL at $T = 10$ K and room temperature [see Figs. 4(a) and 4(b), respectively]. The emission from the thermalized states is observed at 440 nm for higher excitation densities. In contrast to the thin or intermediate thick QW, this QW emission peak at 448 nm does not shift at all. While emission is strong in the screened case, the radiative recombination rate is very low as soon as the field is partially unscreened, thus the redshifted emission due to the quantum-confined Stark effect (QCSE) is not observable for the normalized spectra in Fig. 4. Low-power short pulse excitation however verifies that thermalized states at low carrier densities emit in the spectral range below the 450 nm peak, extending down to about 600 nm [11]. Consequently, the broad peak at 431 nm and low carrier densities is assigned to hot carrier emission. This hot carrier emission between the barrier peak at 395 nm and the band edge states of the fully screened QW at 440 nm is also observable at room temperature [see Fig. 4(b)]. Its intensity is reduced with respect to the barrier peak because of the faster intraband recombination at room temperature.

III. SIMULATION OF HOT CARRIER EMISSION SPECTRA

The experimental results are now compared with Schrödinger-Poisson simulations of luminescence of the screened QW in the $k \cdot p$ approximation, by calculating the emission spectrum in thermal equilibrium from the energy-dependent radiative transition rate

$$r(\hbar\omega) = \frac{q_e^2 n_{\mathrm{eff}}\omega}{2\pi^3 d\hbar m_0^2 c^3 \epsilon_0 E_{\mathrm{hom}}} \sum_{i,j} \iint_{-\infty}^{\infty} |M_{ij}(k_\parallel)|^2 \times f_c(E_{c,i})[1 - f_v(E_{v,j})] \times \mathrm{sech}\left(\frac{E_{c,i} - E_{v,j} - \hbar\omega}{E_{\mathrm{hom}}}\right) \mathrm{d}^2 k_\parallel \quad (1)$$

for the confined states in the conduction and valence bands $E_{c,i}(k_\parallel)$ and $E_{v,j}(k_\parallel)$, depending on the subband index i, j and in-plane momentum $k_\parallel$, with the squared momentum matrix element $|M_{ij}(k_\parallel)|^2$, and occupation of the states given by the Fermi-Dirac distributions f_c, and f_v with quasi-Fermi levels for the valence and conduction band given by carrier density and charge neutrality. This simulation describes the spectra for quasiequilibrium occupation for narrow and wide QWs quantitatively, including the strong redshift, the observation of multiple peaks, and bulklike density of states at low, medium, and high carrier densities, respectively [11].

Hot electron emission can be reproduced by Eq. (1) with two modifications. First, we assume that all states between the band edge and barrier energy levels have equal occupation. This corresponds to the assumption of a relaxation rate with a weak dependency on the subband energy level. For phonon scattering and a weakly varying density of states for confined

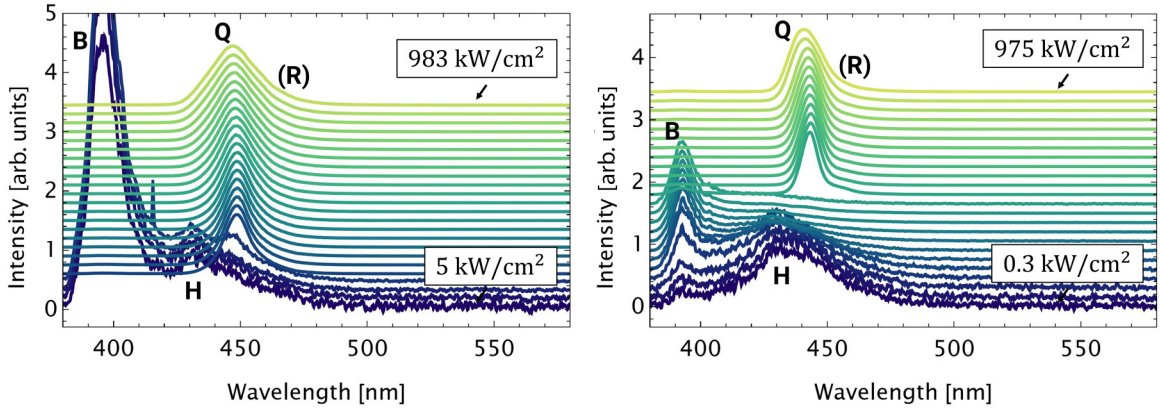


FIG. 4. PL spectra at (a) $T = 10$ K and (b) room temperature for different excitation densities for a 25-nm QW. The spectra are normalized and vertically shifted for clarification. Components of the emission spectrum are marked as B: barrier, H: hot carrier, Q: quantum well, R: phonon replica. The excitation power in (a) is 5 kW/cm^2 $\cdot$ 1.61^i with $i = 0, 1, 2, \ldots, 4$ for the first five spectra and 36.9 kW/cm^2 $\cdot$ 1.2^i with $i = 0, 1, 2, \ldots, 18$ for the remaining spectra and in (b) 0.3 kW/cm^2 $\cdot$ 1.54^i with $i = 0, 1, 2, \ldots, 11$ for the first 12 spectra and 33.1 kW/cm^2 $\cdot$ 1.36^i with $i = 0, 1, 2, \ldots, 11$ for the remaining spectra.

states far above the ground state, this assumption may be justified. Second, we assume that the in-plane momentum $k_\parallel$ of the relaxing carriers is limited. The physical argument is that the distribution of carriers in the transport layer of the barriers has limited energy and thus momentum, and that by relaxation through electron-phonon scattering the momentum will in average decrease by scattering towards the Γ point. The only free parameter in the simulation is the choice of the cutoff value for $k_\parallel$, affecting the calculated spectrum.

Simulated and measured spectra are compared in Fig. 5. The simulation at high carrier density uses Eq. (1) with quasiequilibrium carrier distribution and reproduces the emission spectrum from the fully screened QW. For simulations of the partially screened QW, see Ref. [11]. For the simulation at low carrier density, the term $f_c[E_i(\vec{k})]\{1 - f_v[E_f(\vec{k})]\}$ in Eq. (1) was replaced by 1 to simulate the equal occupation of all states. For the integration over in-plane momentum, a cutoff $k_\parallel \leqslant 0.2$ nm^{-1} was used. The tethered markers indicate the oscillator strength of each individual interband transition at the Γ point. Because of the equal occupation and limitation of the range of integration, the envelope of these roughly reproduces the emission spectrum. If the cutoff radius is increased, then the spectrum extends to higher energies, with little change to the low-energy side.

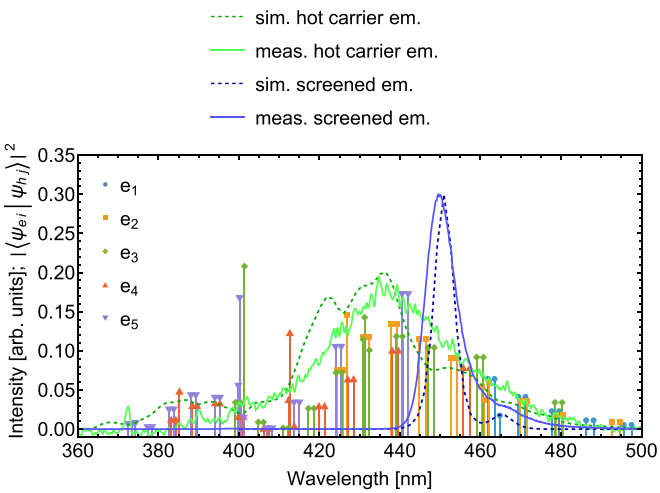


FIG. 5. Simulated transversal electric (TE) spectra at low and high carrier density together with the measured PL spectra for sample PL7.8nm at excitation power densities of 425 and 17 kW/cm^2 at $T = 10$ K. For the low carrier density, the electron-hole wavefunction overlap $|\langle\Psi_{ei}|\Psi_{hj}\rangle|^2$ for all Γ point interband transitions are indicated by the symbols. The simulation at high carrier density ($n = 10^{13}$ cm^{-2}) assumes quasiequilibrium [Eq. (1)], for the low carrier density equal occupation of all states, and a cutoff value 0.2 nm^{-1} for $k_\parallel$ is used.

The assumption of equal occupation of all states underestimates the occupation of the lowest confined states, which are however dark states and do not show up in the spectrum. While the two basic assumptions result in a fair reproduction of the observed spectra, it would be worth to simulate the hot carrier luminescence with advanced simulation methods, employing microscopic models for electron-phonon scattering, as multiscale transport models [36].

IV. CONCLUSION

Luminescence from hot carriers was observed in PL and EL spectra for wide InGaN QWs. The luminescence stems from the interband transition of carriers while they are relaxing by intraband scattering processes from the transport layer towards the QW band edge in the conduction and valence band. Confined states which are in thermal equilibrium at the respective band edge become dark states because of the extremely small overlap of carrier wave functions and do not contribute to the spectrum. For the thermalized state the occupation is high but the transition matrix element is low, while for the hot carriers it is the opposite. This is the condition for the observation of luminescence from hot carriers. With increasing carrier density and thus screening, emission from thermalized states becomes fast and the longer wavelength

peak dominates the spectrum, with emission from hot carriers being negligible in comparison to emission from thermalized carriers. This is the standard case for PL emission. Luminescence from hot carriers was detected for 7.8- and 25-nm-wide QWs at low temperature and for the 25-nm-wide QWs also at room temperature. The shape of the emission spectrum was explained by a modified equation for energy-dependent radiative recombination, making two physically reasoned assumptions: first, an equal occupation of all involved subband states in the flow equilibrium; and second, a cutoff radius for the in-plane momentum of carriers involved in carrier injection.

ACKNOWLEDGMENTS

We would like to thank Carsten Deibel, Jens W. Tomm, and Witold Trzeciakowski for the discussion of the manuscript. This work was funded by the Deutsche Forschungsgemeinschaft (DFG, German Research Foundation) 544925332.

DATA AVAILABILITY

The data that support the findings of this article are openly available [37], embargo periods may apply.

[1] H. Kroemer, Nobel lecture: Quasielectric fields and band offsets: teaching electrons new tricks, Rev. Mod. Phys. **73**, 783 (2001).

[2] Z. I. Alferov, Nobel lecture: The double heterostructure concept and its applications in physics, electronics, and technology, Rev. Mod. Phys. **73**, 767 (2001).

[3] *Quantum Well Lasers. II*, edited by P. S. Zory (Academic Press, San Diego, 1993).

[4] S. Nakamura, M. Senoh, N. Iwasa, and S. Nagahama, High-power InGaN single-quantum-well-structure blue and violet light-emitting diodes, Appl. Phys. Lett. **67**, 1868 (1995).

[5] S. Nakamura, InGaN-based violet laser diodes, Semicond. Sci. Technol. **14**, R27 (1999).

[6] N. F. Gardner, G. O. Müller, Y. C. Shen, G. Chen, S. Watanabe, W. Götz, and M. R. Krames, Blue-emitting InGaN-GaN double-heterostructure light-emitting diodes reaching maximum quantum efficiency above 200 A/cm^{-2}, Appl. Phys. Lett. **91**, 243506 (2007).

[7] A. David and M. J. Grundmann, Droop in InGaN light-emitting diodes: A differential carrier lifetime analysis, Appl. Phys. Lett. **96**, 103504 (2010).

[8] A. Laubsch, M. Sabathil, J. Baur, M. Peter, and B. Hahn, High-power and high-efficiency InGaN-based light emitters, IEEE Trans. Electron Devices **57**, 179 (2010).

[9] G. Muziol, H. Turski, M. Siekacz, K. Szkudlarek, L. Janicki, M. Baranowski, S. Zolud, R. Kudrawiec, T. Suski, and C. Skierbiszewski, Beyond quantum efficiency limitations originating from the piezoelectric polarization in light-emitting devices, ACS Photonics **6**, 1963 (2019).

[10] M. Hajdel, M. Chlipała, M. Siekacz, H. Turski, P. Wolny, K. Nowakowski-Szkudlarek, A. Feduniewicz-Żmuda, C. Skierbiszewski, and G. Muziol, Dependence of InGaN quantum well thickness on the nature of optical transitions in LEDs, Materials **15**, 237 (2021).

[11] L. Uhlig, J. Tepaß, M. Hajdel, G. Muziol, and U. T. Schwarz, Transition between quantum confinement and bulklike behavior in polar quantum wells, Phys. Rev. B **108**, 045304 (2023).

[12] G. Muziol, M. Hajdel, M. Siekacz, K. Szkudlarek, S. Stanczyk, H. Turski, and C. Skierbiszewski, Optical properties of III-nitride laser diodes with wide InGaN quantum wells, Appl. Phys. Express **12**, 072003 (2019).

[13] S.-H. Park, Intraband relaxation time in wurtzite InGaN/GaN quantum-well structures with $(10\bar{1}0)$ crystal orientation, Appl. Phys. Lett. **80**, 2830 (2002).

[14] A. Shikanai, K. Kojima, K. Omae, Y. Kawakami, Y. Narukawa, T. Mukai, and S. Fujita, The hot carrier dynamics in InGaN multi-quantum well structure, Phys. Stat. Sol. (b) **240**, 392 (2003).

[15] K. Kojima, A. Shikanai, K. Omae, M. Funato, Y. Kawakami, Y. Narukawa, T. Mukai, and Sg. Fujita, Optically pumped lasing and gain formation properties in blue $In_xGa_{1-x}N$ MQWs, Phys. Stat. Sol. (b) **241**, 2676 (2004).

[16] J. Seo Im, H. Kollmer, J. Off, A. Sohmer, F. Scholz, and A. Hangleiter, Reduction of oscillator strength due to piezoelectric fields in GaN/$Al_xGa_{1-x}N$ quantum wells, Phys. Rev. B **57**, R9435(R) (1998).

[17] T. F. K. Weatherley, W. Liu, V. Osokin, D. T. L. Alexander, R. A. Taylor, J.-F. Carlin, R. Butté, and N. Grandjean, Imaging nonradiative point defects buried in quantum wells using cathodoluminescence, Nano Lett. **21**, 5217 (2021).

[18] T. Takeuchi, S. Sota, M. Katsuragawa, M. Komori, H. Takeuchi, H. Amano, and I. Akasaki, Quantum-confined Stark effect due to piezoelectric fields in GaInN strained quantum wells, Jpn. J. Appl. Phys. **36**, L382 (1997).

[19] T. Takeuchi, C. Wetzel, S. Yamaguchi, H. Sakai, H. Amano, I. Akasaki, Y. Kaneko, S. Nakagawa, Y. Yamaoka, and N. Yamada, Determination of piezoelectric fields in strained GaInN quantum wells using the quantum-confined Stark effect, Appl. Phys. Lett. **73**, 1691 (1998).

[20] T. Kuroda, A. Tackeuchi, and T. Sota, Luminescence energy shift and carrier lifetime change dependence on carrier density in $In_{0.12}Ga_{0.88}N/In_{0.03}Ga_{0.97}$ quantum wells, Appl. Phys. Lett. **76**, 3753 (2000).

[21] E. Kuokstis, J. W. Yang, G. Simin, M. A. Khan, R. Gaska, and M. S. Shur, Two mechanisms of blueshift of edge emission in InGaN-based epilayers and multiple quantum wells, Appl. Phys. Lett. **80**, 977 (2002).

[22] Y. C. Chow, T. Tak, F. Wu, J. Ewing, S. Nakamura, S. P. DenBaars, Y.-R. Wu, C. Weisbuch, and J. S. Speck, Origins of the high-energy electroluminescence peaks in long-wavelength (∼495–685 nm) InGaN light-emitting diodes, Appl. Phys. Lett. **123**, 091103 (2023).

[23] A. Bercha, G. Muziol, M. Chlipala, and W. Trzeciakowski, Long-lived excitations in wide (In,Ga)N/GaN quantum wells, Phys. Rev. Appl. **20**, 034040 (2023).

[24] J. W. Tomm, A. Bercha, G. Muzioł, J. Piprek, and W. Trzeciakowski, Recombination in polar InGaN/GaN LED structures with wide quantum wells, Phys. Status Solidi RRL **17**, 2300027 (2023).

[25] S. Schmitt-Rink, D. S. Chemla, and D. A. B. Miller, Linear and nonlinear optical properties of semiconductor quantum wells, Adv. Phys. **38**, 89 (1989).

[26] P. Farr, S. Sidikejiang, P. Horenburg, H. Bremers, U. Rossow, and A. Hangleiter, Unity quantum efficiency in III-nitride quantum wells at low temperature: Experimental verification by time-resolved photoluminescence, Appl. Phys. Lett. **119**, 011106 (2021).

[27] A. P. Demchenko, V. I. Tomin, and P.-T. Chou, Breaking the Kasha rule for more efficient photochemistry, Chem. Rev. **117**, 13353 (2017).

[28] J. Iveland, L. Martinelli, J. Peretti, J. S. Speck, and C. Weisbuch, Direct measurement of Auger electrons emitted from a semiconductor light-emitting diode under electrical injection: identification of the dominant mechanism for efficiency droop, Phys. Rev. Lett. **110**, 177406 (2013).

[29] M. Binder, A. Nirschl, R. Zeisel, T. Hager, H.-J. Lugauer, M. Sabathil, D. Bougeard, J. Wagner, and B. Galler, Identification of nnp and npp Auger recombination as significant contributor to the efficiency droop in (GaIn)N quantum wells by visualization of hot carriers in photoluminescence, Appl. Phys. Lett. **103**, 071108 (2013).

[30] T. Brazzini, M. A. Casbon, H. Sun, M. J. Uren, J. Lees, P. J. Tasker, H. Jung, H. Blanck, and M. Kuball, Electroluminescence of hot electrons in AlGaN/GaN high-electron-mobility transistors under radio frequency operation, Appl. Phys. Lett. **106**, 213502 (2015).

[31] I. Rossetto, M. Meneghini, A. Tajalli, S. Dalcanale, C. De Santi, P. Moens, A. Banerjee, E. Zanoni, and G. Meneghesso, Evidence of hot-electron effects during hard switching of AlGaN/GaN HEMTs, IEEE Trans. Electron Devices **64**, 3734 (2017).

[32] H. Turski, G. Muziol, P. Wolny, S. Grzanka, G. Cywiński, M. Sawicka, P. Perlin, and C. Skierbiszewski, Cyan laser diode grown by plasma-assisted molecular beam epitaxy, Appl. Phys. Lett. **104**, 023503 (2014).

[33] C. Becht, U. T. Schwarz, M. Binder, and B. Galler, Diffusion analysis of charge carriers in InGaN/GaN heterostructures by microphotoluminescence, Phys. Status Solidi B **260**, 2200565 (2023).

[34] X. B. Zhang, T. Taliercio, S. Kolliakos, and P. Lefebvre, Influence of electron-phonon interaction on the optical properties of III nitride semiconductors, J. Phys.: Condens. Matter **13**, 7053 (2001).

[35] M. Chlipala, H. Turski, M. Siekacz, K. Pieniak, K. Nowakowski-Szkudlarek, T. Suski, and C. Skierbiszewski, Nitride light-emitting diodes for cryogenic temperatures, Opt. Express **28**, 30299 (2020).

[36] F. Römer, G. Hofmann, J. Höpfner, M. Schilling, A. Muhin, T. Wernicke, M. Kneissl, and B. Witzigmann, Carrier transport in a deep ultraviolet mixed quantum well light emitting diode, IEEE Photonics J. **16**, 8200106 (2024).

[37] U. Schwarz, Raw data for Fig. 2 to Fig. 4 for manuscript "Luminescence from hot carrier interband recombination in wide InGaN quantum wells" by Conny Becht *et al.* [Data set], Zenodo (2025), https://doi.org/10.5281/zenodo.15781403.